Development 140, 3997-4007 (2013) doi:10.1242/dev.091934

Daam1a mediates asymmetric habenular morphogenesis by regulating dendritic and axonal outgrowth

Alicia Colombo[1,*], Karina Palma[1,2], Lorena Armijo[1,2], Marina Mione[3], Iskra A. Signore[1,2], Camila Morales[1], Néstor Guerrero[1,2], Margarita M. Meynard[1,2], Ramón Pérez[1,2], José Suazo[4], Katherine Marcelain[1], Luis Briones[1,2], Steffen Härtel[1,2], Stephen W. Wilson[5] and Miguel L. Concha[1,2,*]

SUMMARY

Although progress has been made in resolving the genetic pathways that specify neuronal asymmetries in the brain, little is known about genes that mediate the development of structural asymmetries between neurons on left and right. In this study, we identify *daam1a* as an asymmetric component of the signalling pathways leading to asymmetric morphogenesis of the habenulae in zebrafish. Daam1a is a member of the Formin family of actin-binding proteins and the extent of Daam1a expression in habenular neuron dendrites mirrors the asymmetric growth of habenular neuropil between left and right. Local loss and gain of Daam1a function affects neither cell number nor subtype organisation but leads to a decrease or increase of neuropil, respectively. Daam1a therefore plays a key role in the asymmetric growth of habenular neuropil downstream of the pathways that specify asymmetric cellular domains in the habenulae. In addition, Daam1a mediates the development of habenular efferent connectivity as local loss and gain of Daam1a function impairs or enhances, respectively, the growth of habenular neuron terminals in the interpeduncular nucleus. Abrogation of Daam1a disrupts the growth of both dendritic and axonal processes and results in disorganised filamentous actin and α-tubulin. Our results indicate that Daam1a plays a key role in asymmetric habenular morphogenesis mediating the growth of dendritic and axonal processes in dorsal habenular neurons.

KEY WORDS: Asymmetry, Nervous system, Morphogenesis, Daam1, Habenula, Zebrafish

INTRODUCTION

Neuroanatomical and functional differences between the left and right sides of the nervous system are conserved and crucial features that offer selective advantages for neuronal computation and behavioural performance (Concha et al., 2012). One central question that has engaged the attention of investigators for years is how asymmetric circuits develop in the embryonic nervous system. In vertebrates, this question has begun to be systematically addressed using zebrafish, a model organism that besides offering general advantages for genetic manipulation and direct visualisation of developmental processes, also reveals conspicuous asymmetries in the diencephalic epithalamus (Concha, 2004; Concha et al., 2009; Roussigne et al., 2011). The epithalamic region is formed by two main neuronal groups: the pineal complex (composed of pineal and parapineal nuclei) and the habenula (Hb) (Concha and Wilson, 2001). Among these nuclei, the Hb functions as a relay station that links limbic and striatal forebrain nuclei to monoaminergic systems of the ventral midbrain (Bianco and Wilson, 2009; Aizawa et al., 2011). In zebrafish, the Hb comprises dorsal (d-Hb) and ventral (v-Hb) domains that are homologous to the medial and lateral Hb of mammals, respectively (Aizawa et al., 2005; Aizawa et al., 2011). In contrast to mammals, the zebrafish d-Hb develops pronounced cellular and molecular asymmetries from about 36 hours post-fertilisation (hpf) that appear to rely on lateralised differences in the timing of neurogenesis (Aizawa et al., 2007). Such genetically encoded asymmetries are proposed to depend, at least in part, on early interactions established between the Hb and the left-sided-positioned parapineal nucleus (Concha et al., 2003; Gamse et al., 2003; Bianco et al., 2008), and results in the asymmetric organisation of molecular markers that define lateral (d-Hb_L) and medial (d-Hb_M) cellular subdomains of the d-Hb (Gamse et al., 2003; Aizawa et al., 2005; Agetsuma et al., 2010). One important additional feature exhibited by unipolar neurons of the d-Hb_L and d-Hb_M is their distinct axonal terminal morphology and target selectivity for dorsal and ventral domains of the interpeduncular nucleus (IPN) (Gamse et al., 2003; Aizawa et al., 2005; Bianco et al., 2008). As a consequence of such selectivity and the asymmetric organisation of d-Hb_L and d-Hb_M domains, neuronal projections from the left (primarily d-Hb_L) and right (primarily d-Hb_M) are largely segregated within dorsal and ventral domains of the IPN, respectively (Aizawa et al., 2005; Gamse et al., 2005), and this distinctive neuronal substrate appears to have important roles in the modulation of behavioural responses to fear, anxiety and stress-inducing stimuli (Facchin et al., 2009; Agetsuma et al., 2010; Lee et al., 2010; Jesuthasan, 2011).

Besides the observed cellular and molecular asymmetries, the zebrafish d-Hb also develops structural asymmetries in the size and organisation of neuropil domains (Concha et al., 2000) within which dendritic extensions from habenular neurons mix and synapse with axonal afferents arriving from other regions of the forebrain through the stria medullaris (Hendricks and Jesuthasan, 2007a; Bianco et al., 2008; Miyasaka et al., 2009). Habenular neuropil formation begins at ~48 hpf, subsequent to the specification of d-Hb_L and d-Hb_M cellular domains, and becomes progressively enlarged on the

[1]Institute of Biomedical Sciences, Facultad de Medicina, Universidad de Chile, Independencia 1027, Santiago 8380453, Chile. [2]Biomedical Neuroscience Institute, Universidad de Chile, Independencia 1027, Santiago 8380453, Chile. [3]Karlsruhe Institute of Technology, Hermann-von-Helmholtz-Platz 1, 76344 Eggenstein-Leopoldshafen, Germany. [4]Department of Nutrition, Diabetes and Metabolism, Facultad de Medicina, Pontificia Universidad Católica de Chile, Santiago 8331150, Chile. [5]Department of Cell and Developmental Biology, University College London, Gower Street, London WC1E 6BT, UK.

*Authors for correspondence (acolombo@med.uchile.cl; mconcha@med.uchile.cl)

Accepted 8 July 2013

left side reaching a conspicuous asymmetric array by 4 days of development (Concha et al., 2000; Concha et al., 2003). Importantly, organisation of neuropil asymmetry resembles the asymmetric distribution of *kctd12.1* transcripts (Gamse et al., 2003), suggesting a causative link between neuropil organisation and the asymmetric distribution of cell subtypes in the d-Hb. Consistent with this idea, loss or gain of Kctd12.1 function affects habenular neuropil formation (Taylor et al., 2011), and the asymmetry of habenular neuropil becomes disrupted in conditions that affect the asymmetric expression of *kctd12.1*, such as after ablation of the parapineal nucleus (Concha et al., 2003; Bianco et al., 2008) and in mutants with defective Fibroblast growth factor 8 (Fgf8) (*acerebellar*$^{-/-}$, *ace*$^{-/-}$) (Regan et al., 2009) or Wnt/β-catenin (*masterblind*$^{-/-}$, *mbl*$^{-/-}$) (Carl et al., 2007) signalling. In these cases, the d-Hb develops into an almost bilaterally symmetric structure.

Despite our growing understanding of the signalling events that specify neuronal asymmetries in the d-Hb, we still know very little about how structural asymmetries in neuropil distribution arise. In this study, we identify a novel genetic component of the pathways that control asymmetric neuropil formation in the d-Hb of zebrafish. *dishevelled associated activator of morphogenesis 1a* (*daam1a*) was isolated from a reverse genetic screen searching for genes differentially expressed in left and right sides of the zebrafish brain. *daam1a* encodes a Diaphanous-related formin (Drf) protein that belongs to the phylogenetically conserved Formin family of actin assembly factors (Wallar and Alberts, 2003). The extent of Daam1a expression matches the asymmetric growth of habenular neuropil during embryonic and larval stages of zebrafish. Local loss and gain of Daam1a function in the left Hb prior to the onset of neuropil formation results in decreased or increased left habenular neuropil, respectively, without affecting neurogenesis or cell subtype specification. At the level of single habenular neurons, knockdown of Daam1a results in impaired growth of both dendritic and axonal extensions. Our results indicate that Daam1a is a key modulator of asymmetric habenular morphogenesis, mediating the outgrowth of dendritic and axonal processes in dorsal habenular neurons.

MATERIALS AND METHODS

Zebrafish lines

Embryos of zebrafish (*Danio rerio*) were obtained by natural spawning, raised at 28°C in embryo medium and staged according to morphology (Kimmel et al., 1995) and age (hours and days post-fertilisation; hpf and dpf). Zebrafish lines used were: wild-type Tübingen, *Tg(foxD3:GFP)* (Gilmour et al., 2002), *Tg(pou4f1-hsp70l:GFP)* (Aizawa et al., 2005), *Tg(ET16:GFP)* (Parinov et al., 2004), *acerebellar*^{ti282} (Reifers et al., 1998) and *masterblind*^{tm213} (Heisenberg et al., 2001). All animal protocols were approved by the Bioethics Committee of the Faculty of Medicine, University of Chile.

Suppression subtractive hybridisation and screening of differentially expressed clones

Right (R) and left (L) halves of juvenile (1-month-old) zebrafish brains were microdissected, mRNA isolated with Oligotex Direct mRNA Kit (QIAGEN) and cDNA synthesised by the Gubler–Hoffman method (Gubler and Hoffman, 1983). Suppression subtractive hybridisation (SSH) was performed using the PCR-Select cDNA Subtraction Kit (BD Biosciences-Clontech). For direct SSH, R cDNA was used as tester with L cDNA as driver (R-L) and the opposite was used for reverse SSH (L-R). Amplified R and L cDNAs were labelled with [α^{32}P] dCTP by random priming (Prime-a-Gene Labelling System, Promega) and used as probes to hybridise zebrafish cDNA commercial libraries: 611 Zebrafish Brain cDNA pt.2 330.1.545, 611 Zebrafish Brain cDNA pt.1 330.1.521 and 609 Zebrafish EST pt.1.357.1.512 (RZPD). Differential clones were sequenced and analysed *in silico* (www.ncbi.nlm.nih.gov, www.ensembl.org).

Quantitative real-time PCR

Total RNA was isolated from three independent pools of ten L and ten R halves of zebrafish brains, and cDNA generated using SuperScript II Reverse Transcriptase (Invitrogen). Primers used were: 5′-GGAGGTCATGGCGCGTCC-3′ (sense) and 5′-CCTCCCGAAGACGGTAGGTG-3′ (antisense) for *daam1a*; 5′-AGTTCTTTCAGCTGCGGGACCTTA-3′ (sense) and 5′-GCGACGGACAGTGTGCGAGAG-3′ (antisense) for *kctd12.1*; 5′-AGCTGTTTTAGATGGGGTGTTGTC-3′ (sense) and 5′-AATGTCCTGGTTCTGCCTTAC-3′ (antisense) for *cpd2* (*cadps2*); and 5′-GGCACCGGTTCTGGCTTCAC-3′ (sense) and 5′-CGGAGATCACTGGGGCATAGGTA-3′ (antisense) for *α-tubulin* (control). Quantitative PCR was carried out on a 7300 real-time PCR system (Applied Biosystems, Carlsbad, CA, USA) with Platinum SYBR Green qPCR Supermix-UDG (Invitrogen). Data were compiled and collected using MxPro QPCR (Agilent Technologies), and presented as the fold change in gene expression normalised to *α-tubulin* and expressed as L relative to R or R relative to L. Relative fold changes were calculated by a comparative C (T) method (Schmittgen and Livak, 2008).

Whole-mount *in situ* hybridisation, immunofluorescence and nuclear staining

Whole-mount *in situ* hybridisation was performed as described (Thisse and Thisse, 2008) using antisense probes for *kctd12.1*, *pou4f1* (Aizawa et al., 2005), *lefty1* (Bisgrove et al., 1999), *southpaw* (Long et al., 2003) and *pitx2* (Essner et al., 2000). Antisense *daam1a* was synthesised from the partial coding sequence contained in a commercial clone (UCDMp611A02132Q14, RZPD). The anti-Daam1 antibody (Abnova, 1:50) (Liu et al., 2008) recognised 111 amino acids of the N-terminal region of the human DAAM1, which shares 84% identity with the zebrafish Daam1a protein. For anti-Daam1 and anti-GFP (Invitrogen, 1:1000), fixed embryos were treated with 1 mg/ml collagenase (Sigma) (Burgess et al., 2009). Immunostaining for anti-acetylated α-tubulin (Sigma-Aldrich, 1:1000) was performed as described (Concha et al., 2003). For anti-α-tubulin (Sigma, 1:50) and Alexa Fluor 568 phalloidin (Invitrogen, 1:200), embryos were fixed in 3.7% formaldehyde (Merck) in 0.8% MeOH/PBS, or in 4% paraformaldehyde (PFA) (Polysciences). Alexa Fluor 488-, 568- and 647-conjugated secondary antibodies were used (Invitrogen, 1:200). For nuclear counterstaining, embryos were incubated at 4°C with NeuroTrace 488 green Nissl (Molecular Probes, 1:250) (Signore et al., 2009) and TO-PRO-3 iodide stain (642/661) (Molecular Probes, 1:1000) (Regan et al., 2009).

Morpholino antisense oligonucleotide injection and rescue assays

Antisense morpholino oligonucleotides (MOs) against *southpaw* (*spaw-MO*, 10 ng/embryo) (Long et al., 2003), *no tail* (*ntl-MO*, 1.8 ng/embryo) (Feldman and Stemple, 2001), *ulk2* (*ulk2*^{spl}*-MO*, 2 ng/embryo) (Taylor et al., 2011) and *daam1a* (*daam1a-MO*; 8 ng/embryo; 5′-AGCTATGACCCCCTCTCAAAATGGC-3′, tagged with lissamine at the 3′) (Kida et al., 2007), and control morpholino (Co-MO, 8 ng/embryo; 5′-AGCTATGACCCCCTCTCAAAATGGC-3′, tagged with lissamine at the 3′) were injected in one- to four-cell zebrafish embryos using standard procedures. Efficiency of gene knockdown was assessed by phenotype, epithalamic *lefty1* expression (absent in *spaw-MO* and bilateral in *ntl-MO*), or Daam1a immunostaining (reduced in *daam1a-MO*). *pCS2-GFP-hDaam1* and unc-51-like kinase (ulk2) [gifts from Drs R. Habas (College of Science and Technology, Temple University, Philadelphia, PA, USA) and J. Gamse (Medical Center, Vanderbilt University, Nashville, TN, USA), respectively] were used for standard mRNA *in vitro* synthesis. For rescue experiments, embryos were co-injected with one of the following combinations: 200 pg *GFP-hDAAM1* mRNA + 8 ng *daam1a-MO*; 200 pg *GFP-hDAAM1* mRNA + 8 ng Co-MO; 200 pg *GFP-hDAAM1* mRNA + 2 ng *ulk2*^{spl}*-MO*; 150 pg *ulk2* mRNA + 2 ng *ulk2*^{spl}*-MO*; or 150 pg *ulk2* mRNA + 8 ng *daam1a-MO*.

Local and focal electroporation

Focal electroporation was performed as described (Tawk et al., 2009) using *pCS2-GAP43-mCherry* or *pCS2-GAP43-GFP* plasmids. Local electroporation was adapted from a previous report (Hendricks and Jesuthasan, 2007b). In brief, glass injection needles were filled with *daam1a-MO* (1 mM), Co-MO (1 mM), *pcDNA-C-DAAM1-HA* (1.5-2

µg/µl) or *pCS2-GAP43-GFP* (1.5-2 µg/µl). MO or DNA was injected into the third ventricle using a Picospritzer III (Parker Hannifin). Five 25-volt pulses, each lasting 1 msecond, were manually applied at 20 Hz using a Grass DS9 stimulator.

Labelling of habenular efferent projections

Larvae were fixed in 4% PFA in PBS and the skin covering the dorsal diencephalon and eyes was removed. Crystals of the lipophilic dyes DiD and DiO (Molecular Probes) were applied to L and R Hb, respectively, using tungsten needles connected to a micromanipulator (Aizawa et al., 2005; Signore et al., 2009). Labelled larvae were incubated in 0.5% PFA in PBS at 48°C for 2 days in the darkness, to allow lipophilic dyes to reach the IPN.

Confocal image acquisition and processing

Embryos were anaesthetised (0.003% tricaine), mounted in 1% low melting agarose and imaged as described (Concha et al., 2003; Signore et al., 2009) using UltraView RS spinning disc microscope (PerkinElmer) with C-Apochromat 40×/1.2 W or 63×/1.2 W, or Fluoview1000 Spectral confocal microscope (Olympus) with Plan-Apochromat 40×/1.0 W. Images were deconvolved to reduce blurring and noise (Huygens Professional, SVI) and optimised for brightness/contrast keeping the dynamic range of raw images. 3D image projections were obtained using Volocity (PerkinElmer), ImageJ (http://rsbweb.nih.gov/ij/) and SCIAN-Soft (http://www.scian.cl). Final figure panels were selected according to both consensus criteria and representative phenotype.

Quantification of cell number, neuropil and IPN volume

The number of HuC (Elavl3)- and HuD (Elavl4)-positive (+) nuclei in the Hb labelled by anti-HuC/D immunostaining (Invitrogen, 1:500) was determined from confocal image *z*-stacks as described (Roussigné et al., 2009). Volume was measured in 3D reconstructions using custom-made image-processing routines written in SCIAN-Soft, which involved thresholding, manual and automated segmentation, and generation of binary masks of the habenular neuropil and IPN.

Statistics

Statistical analyses were performed using Origin Pro8 software. Comparison of individual datasets from different conditions was performed using the Kolmogorov–Smirnov (KS) test. A *t*-test was used to compare differences in IPN volume. The Mann–Whitney non-parametric test was used to compare differences in neuropil volume and values of L-R gene expression obtained by qPCR. Significance was set at $P<0.05$.

RESULTS

A subtractive hybridisation approach identified *daam1a* as a gene enriched on the left side of the zebrafish brain

To identify genes with asymmetric expression in the zebrafish brain, cDNAs obtained through reverse transcription of mRNA samples

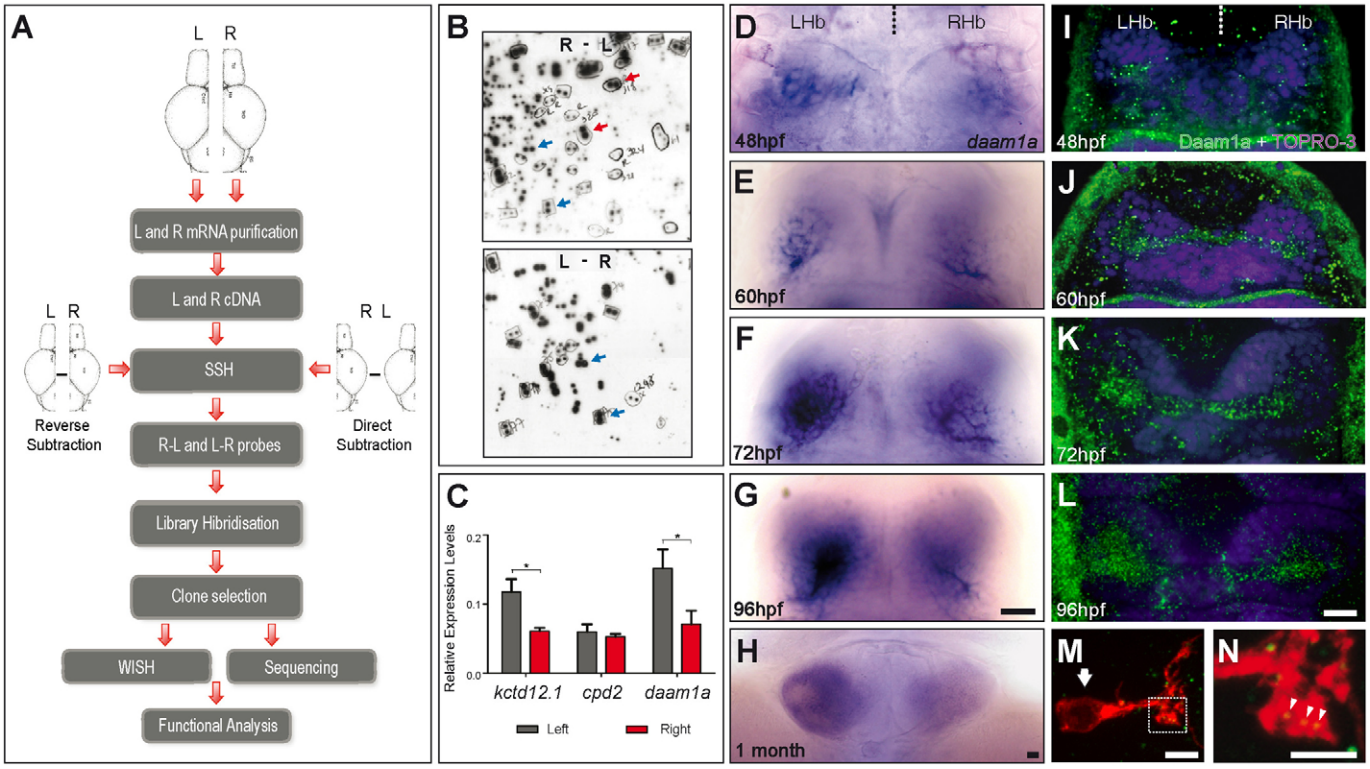

Fig. 1. Identification of *daam1a* as a novel gene with asymmetric expression in the zebrafish brain. (**A**) Strategy for the identification of sequences differentially expressed in left and right sides of the juvenile zebrafish brain. For details, see text. (**B**) Radioautography images obtained after library hybridisation with probes obtained from direct (top) and reverse (bottom) SSH. Arrows indicate examples of selected clones hybridised by a single SSH condition (red), or showing differential hybridisation intensity between both conditions (blue). (**C**) Quantitative assessment of *kctd12.1* (control asymmetric gene enriched on the left side), *cpd2* (control symmetric gene) and *daam1a* mRNA expression in left (grey) and right (red) halves of juvenile brains. Asterisks indicate statistically significant differences between left and right brain ($n=10$), after Mann–Whitney test: *kctd12.1* ($P<0.004$); *daam1a* ($P<0.025$). Error bars represent standard errors. (**D-H**) Expression of *daam1a* mRNA after whole-mount *in situ* hybridisation in embryonic (D-F), larval (G) and juvenile (H) zebrafish. (**I-L**) Expression of Daam1a protein visualised by confocal microscopy after whole-mount indirect immunofluorescence (green) in embryonic (I-K) and larval (L) zebrafish. TO-PRO-3 was used as nuclear counterstain (purple). Images in D-L are dorsal views, with anterior to the top. (**M**,**N**) Maximum intensity confocal projections showing a single habenular neuron labelled through focal electroporation of *pCS2-GAP43-mCherry* (red) and immunostained against Daam1a (green). The arrow in M indicates the neuronal soma. The punctate distribution of Daam1a in dendrites is shown by arrowheads in panel N, which corresponds to a magnification view of the boxed region in M. L, left; LHb, left Hb; R, right; RHb, right Hb. Scale bars: 20 µm (D-L); 4 µm (M,N).

isolated from L and R halves of juvenile brains were used for direct (R-L) and reverse (L-R) SSH (Fig. 1A). Differential cDNA products were used as probes to screen zebrafish cDNA libraries. Library clones that were differentially hybridised by probes from either direct or reverse SSH but not both, and those for which strength of hybridisation significantly differed between the two SSH conditions (Fig. 1B), were chosen for further *in silico* analysis and assessment of mRNA expression through whole-mount *in situ* hybridisation. We identified *daam1a* as a gene enriched on the left side of the zebrafish brain. qPCR analysis corroborated the presence of higher levels of *daam1a* mRNA in the L compared with the R side of juvenile brains (Mann–Whitney test, $P<0.025$) (Fig. 1C).

Daam1a is expressed in the asymmetric neuropil of the developing dorsal habenula

daam1a mRNA was detected in a distinct domain of the d-Hb that is larger on the L than on the R. Asymmetric expression was detected from ~48 hpf (Fig. 1D,E), became conspicuous at 72 hpf (Fig. 1F), and continued throughout larval (Fig. 1G) and juvenile (Fig. 1H) stages into adulthood (data not shown). In the larvae, *daam1a* mRNA localised to the asymmetric habenular neuropil (Fig. 1G). Whole-mount immunofluorescence (using an antibody directed against human DAAM1 that also detects zebrafish Daam1a) (Liu et al., 2008) revealed a modest asymmetric expression of Daam1 at the outset of habenular neuropil formation (Fig. 1I) that progressively increased following the changes in neuropil growth (Fig. 1J-L). At the subcellular level, Daam1a was detected in a punctate pattern that was highly enriched in the habenular neuropil (Fig. 1L) and could be detected in the soma (Fig. 1M, arrow) and dendritic processes (Fig. 1N, arrowheads) of single habenular neurons. Consistent with Daam1a levels mirroring the growth of habenular neuropil, expression of *daam1a* was symmetric in the Hb of *ace*$^{-/-}$ and *mbl*$^{-/-}$ mutants, which develop symmetric habenular neuropil (Carl et al., 2007; Regan et al., 2009) (supplementary material Fig. S1; Table 1). Conditions in which Nodal signalling in the brain is either absent (e.g. after *southpaw* morpholino injection, *spaw-MO*) (Long et al., 2003) or bilateral (e.g. after *no tail* morpholino injection, *ntl-MO*) (Feldman and Stemple, 2001), and which result in randomisation of habenular neuropil asymmetry (Concha et al., 2000; Gamse et al., 2005), also resulted in randomised directionality of *daam1a* asymmetric expression in the Hb (supplementary material Fig. S1; Table 1). Altogether, these results indicate that expression levels of Daam1a mirror the asymmetric growth of habenular neuropil in the Hb, suggesting that Daam1a is a readout of asymmetric habenular morphogenesis.

Global loss of Daam1a function disrupts the development of habenular neuropil and efferent connectivity to the IPN

To investigate a possible role of Daam1a in asymmetric habenular morphogenesis, we initially performed global Daam1a knockdown by injection at the one- to four-cell stage of a morpholino antisense oligonucleotide designed to block *daam1a* translation (*daam1a-MO*) (Kida et al., 2007). Embryos injected with control morpholino (Co-MO) developed a characteristic left-sided enlarged habenular neuropil as assessed by anti-acetylated α-tubulin immunostaining (Fig. 2A, brackets) (Concha et al., 2000; Concha et al., 2003). In addition, axons from habenular neurons labelled with the *pou4f1-hsp70l:GFP* transgene (Aizawa et al., 2005) projected through the fasciculi retroflexus to the IPN, where they organised in a characteristic ring-shape pattern (Fig. 2K). Global loss of Daam1a function induced two main classes of phenotypes in the Hb. First,

Table 1. Expression of *daam1a* and *kctd12.1* in embryos with symmetric and heterotaxic habenular development

			Symmetric (%)			
	L>R (%)	R>L (%)	L	R	Absent (%)	Total (*n*)
southpaw-MO (*spaw-MO*)						
daam1a						
Co-MO	93	7	–	–	–	46
spaw-MO	53	45	–	–	2	38
kctd12.1						
Co-MO	98	2	–	–	–	44
spaw-MO	53	47	–	–	–	30
no tail-MO (*ntl-MO*)						
daam1a						
Co-MO	94	6	–	–	–	31
ntl-MO	42	43	5	–	10	70
kctd12.1						
Co-MO	100	–	–	–	–	44
ntl-MO	55	41	2	–	2	83
acerebellar (*aceti282*$^{-/-}$)						
daam1a						
sibling	96	2	–	-	2	120
aceti282$^{-/-}$	20	3	–	39	35	68
kctd12.1						
sibling	88	6	–	1	5	158
aceti282$^{-/-}$	–	–	–	55	45	130
masterblind (*mbltm213*$^{-/-}$)						
daam1a						
sibling	73	12	–	10	5	61
mbltm213$^{-/-}$	5	3	–	72	20	54
kctd12.1						
sibling	98	–	–	1	–	41
mbltm213$^{-/-}$	6	15	–	68	3	33

L, left; R, right; symmetric L, both sides of the Hb showing left characteristics; symmetric R, both sides of the Hb showing right characteristics.

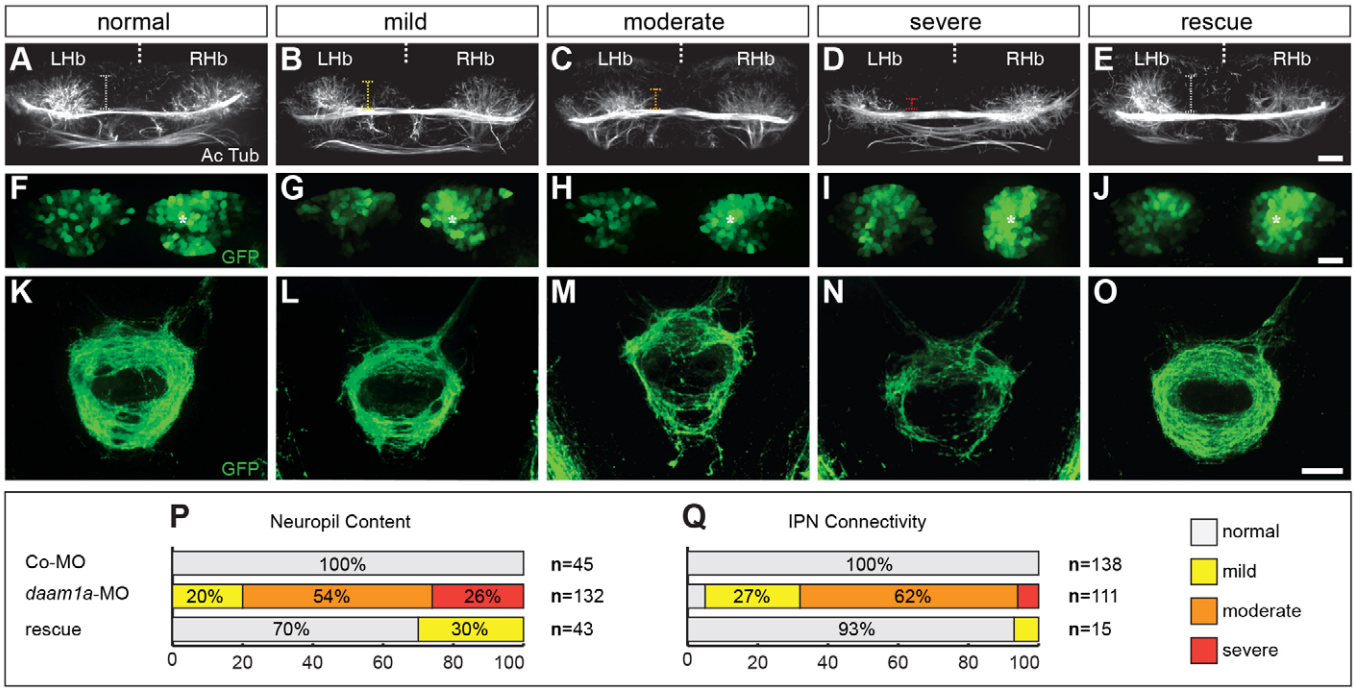

Fig. 2. Global knockdown of Daam1a affects the formation of habenular neuropil and axonal efferent connectivity to the IPN. (**A-O**) Dorsal views of the habenular region (A-J) and IPN (K-O) of *Tg(pou4f1-hsp70l:GFP)* zebrafish at 4.5 dpf, with anterior to the top. The habenular neuropil was immunostained against acetylated α-tubulin (A-E, white), whereas the soma (F-J) and efferent projections (K-O) of dorsal habenular neurons expressing *pou4f1-hsp70l:GFP* were labelled *in vivo* (green). Defects in the Hb and IPN induced by injection of *daam1a-MO* were classified as 'normal', 'mild', 'moderate' or 'severe' phenotypes (columns 1-4). Column 5 (rescue) corresponds to the phenotypes observed after co-expression of *daam1a-MO* and h*DAAM1* mRNA. All images are maximum intensity *z*-stack confocal projections. Vertical dotted brackets in A-E indicate the extent of habenular neuropil in the left Hb. Asterisks in F-J indicate the enlarged cellular domain of the Hb expressing *pou4f1-hsp70l:GFP*. (**P**,**Q**) Distribution of the different phenotypes of habenular neuropil (P) and efferent connectivity to the IPN (Q) in Co-MO, *daam1a-MO* and rescue conditions. Data are presented as the percentage of total larvae showing the indicated phenotype. L, left; LHb, left Hb; R, right; RHb, right Hb. Scale bars: 20 μm.

some *daam1a-MO* embryos (32%; *n*=324) displayed reversed directionality of habenular asymmetry with neuropil in the R Hb showing L-side characteristics and L Hb displaying neuropil properties of the R Hb (Table 2). We found that such complete reversal of neuropil asymmetry was due to an early role of Daam1a in the control of embryo asymmetry, which resulted in disruption of Nodal signalling in both the lateral plate mesoderm and the epithalamus, and subsequently in randomised directionality of epithalamic asymmetry (data not shown).

The second class of habenular phenotype involved a reduction in both the extent of habenular neuropil (Fig. 2B-D, brackets) and the number of habenular axons reaching the IPN (Fig. 2L-N). Most *daam1a-MO* embryos displayed a moderate phenotype in both the Hb (54%; Fig. 2C,P) and the IPN (62%; Fig. 2M,Q). In these cases, which comprised left-sided and reversed phenotypes with mild or moderate neuropil reduction, the pattern of neuropil still remained asymmetric (Fig. 2C); this is in contrast to the most severe phenotypes (26%) in which both sides of the Hb developed a

Table 2. Effects of global knock-down of Daam1a in habenular neuropil asymmetry and in the distribution of genetic markers of the habenulae

	L>R (%)	R>L (%)	Symmetric R (%)	Absent (%)	Total (n)
Neuropil					
Co-MO	96	4	–	–	357
daam1a-MO	37	32	31	–	324
pou4f1-hsp70l:GFP					
Co-MO	4	96	–	–	138
daam1a-MO	35	65	–	–	109
ET16:GFP					
Co-MO	99	1	–	–	54
daam1a-MO	69	30	–	–	59
daam1a					
Co-MO	100	–	-	–	129
daam1a-MO	33	35	32	–	138
kctd12.1					
Co-MO	100	–	–	–	253
daam1a-MO	39	33	28	–	170

L, left; R, right; symmetric R, both sides of the Hb showing right characteristics.

minimal amount of neuropil (Fig. 2D). Co-injection of *daam1a-MO* and human *DAAM1* (h*DAAM1*) mRNA resulted in habenular neuropil and IPN connectivity similar to controls (Fig. 2E,O-Q), indicating that abrogation of Daam1a function was directly responsible for the observed phenotypes. Indeed, functional loss of Daam1a did not disrupt habenular neurogenesis as the number of HuC (+) post-mitotic habenular neurons was similar in control and *daam1a-MO* embryos at 48 hpf (*daam1a-MO*=230±22; Co-MO=234±17; mean±s.d.; $P>0.05$; $n=9$). Specification of habenular cell subtypes was also unaffected as revealed by the normal asymmetric organisation of GFP (+) domains after Daam1a knockdown in two transgenic lines labelling distinct asymmetrically distributed neuronal subtypes of the d-Hb, *Tg(pou4f1-hsp70l:GFP)* (Aizawa et al., 2005) and *Tg(ET16::GFP)* (Parinov et al., 2004) (Fig. 2G-I; Table 2). Furthermore, the parapineal nucleus was lateralised towards the side of enlarged habenular neuropil, and in the most severe neuropil phenotypes (Fig. 2D) the parapineal still adopted a lateral position (data not shown), suggesting that Daam1a knockdown affected events downstream of the pathways that control the lateral positioning of the parapineal nucleus. The only asymmetric habenular marker that was reduced after Daam1a knockdown, other than *daam1a*, was *kctd12.1* (supplementary material Fig. S2; Table 2), which also localises to the habenular neuropil (Gamse et al., 2003). In conclusion, these results indicate that Daam1a is required for habenular asymmetric morphogenesis, in particular for the development of asymmetric neuropil and the establishment of connectivity from the Hb to the IPN.

Habenular knockdown of Daam1a decreases the formation of neuropil and efferent connectivity to the IPN

To verify that Daam1a plays a direct role in neuronal morphogenesis of the Hb, we performed spatio-temporally restricted knockdown of Daam1a through local electroporation of *daam1a-MO* directly into the habenular region at a developmental stage that followed cell subtype specification and preceded the onset of habenular morphogenesis (44 hpf) (Fig. 3A). We focused on targeting the L Hb, as this was the primary site of endogenous

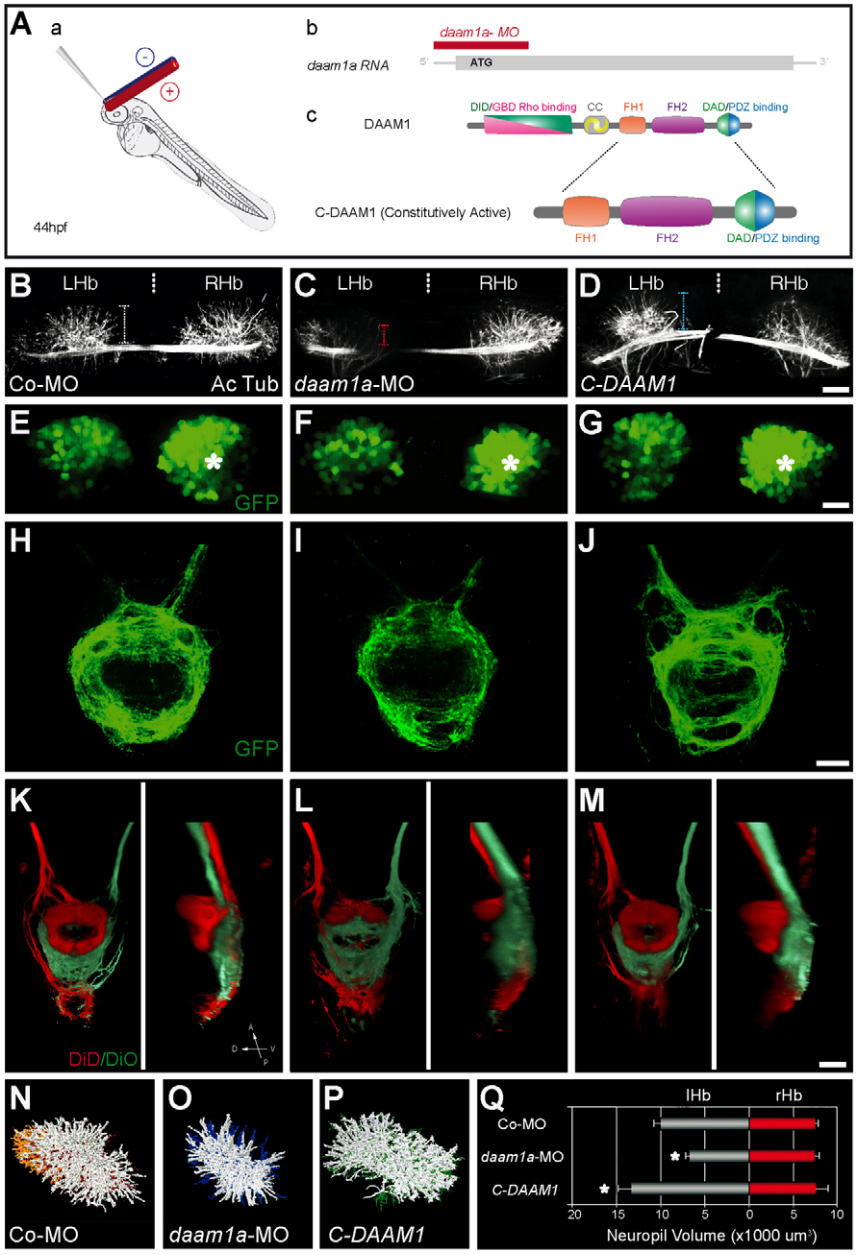

Fig. 3. Local loss and gain of Daam1a function induces opposite modulatory effects in the growth of habenular neuropil and axonal efferent connectivity to the IPN. (**A**) Schematics of the local electroporation procedure (a), *daam1a-MO* design (b) and constitutively active form of C-Daam1a (c). (**B-J**) Dorsal views of the habenular region (B-G) and IPN (H-J) of *Tg(pou4f1-hsp70l:GFP)* zebrafish at 4.5 dpf, with anterior to the top. The habenular neuropil was immunostained against acetylated α-tubulin (B-D, white), whereas the soma (E-G) and efferent projections (H-J) of dorsal habenular neurons expressing *pou4f1-hsp70l:GFP* were labelled *in vivo* (green). Vertical dotted brackets in B-D indicate the extent of neuropil development in the left Hb. Asterisks in E-G indicate the enlarged cellular domain of the Hb expressing *pou4f1-hsp70l:GFP*. (**K-M**) Dorsal (left) and lateral (right) views of the IPN at 4.5 dpf, with anterior to the top, after labelling the left (red) and right (green) Hb with DiD and DiO, respectively. Images in B-M are maximum intensity *z*-stack confocal projections, organised in three columns that correspond to different electroporation conditions: control-MO (left), *daam1a-MO* (middle) and *pcDNA-C-DAAM1-HA* (right). (**N-P**) Dorsal views of three-dimensional volumetric reconstructions of the left habenular neuropil in the three electroporation conditions. (**Q**) Quantification of left (grey) and right (red) habenular neuropil volumes. Asterisks indicate statistically significant decrease (*daam1a-MO*, $n=5$) or increase (*pcDNA-C-DAAM1-HA*, $n=5$) of left habenular neuropil volume with respect to controls (Co-MO, $n=5$; control plasmid, $n=6$), after Mann–Whitney test ($P<0.05$). Error bars represent s.d. D, dorsal; L, left; LHb, left Hb; R, right; RHb, right Hb; V, ventral. Scale bars: 20 μm.

daam1a expression, although we obtained similar results after bilateral electroporation of the Hb (Fig. 3; supplementary material Fig. S5). Local electroporation of *daam1a-MO* efficiently led to both morpholino incorporation (supplementary material Fig. S3) and reduced levels of Daam1a protein expression (supplementary material Fig. S4). Importantly, the extent of neuropil was markedly reduced in the L Hb of *daam1a-MO*-electroporated embryos (Fig. 3C, brackets) compared with controls (Fig. 3B, brackets), similar to the severe phenotypes observed after global knockdown of Daam1a (compare Fig. 3C with Fig. 2D). Indeed, quantification of habenular neuropil volume revealed a significant decrease in the L Hb of electroporated embryos compared with controls (L-Hb-*daam1a-MO*=6752±442 μm^3; L-Hb-Co-MO=10,042±747 μm^3; P<0.05; n=5) (Fig. 3N,O,Q) whereas neuropil of the R Hb remained unaffected (Fig. 3Q). In addition to changes in habenular neuropil, left-sided local electroporation of *daam1a-MO* also induced a decrease in the extent of *pou4f1-hsp70l:GFP* (+) axonal labelling in the IPN (Fig. 3I; supplementary material Fig. S5) and in the volume of L Hb projections reaching the dorsal IPN (dIPN) compared with controls (L-Hb-dIPN-*daam1-MO*=13,001±502 μm^3; L-Hb-dIPN-Co-MO=29,820±1595.4 μm^3; P<0.05; n=4), whereas projections to the ventral IPN (vIPN) from either R or L Hb appeared unaltered (data not shown, P>0.05; n=4) (Fig. 3K,L). As we did not observe axons projecting to ectopic brain regions (data not shown) and the number and organisation of habenular cell subtypes appeared unaffected as revealed by the normal expression of the *pou4f1-hsp70l:GFP* transgene (Fig. 3C,F), we interpreted the loss of IPN connectivity as a primary defect in habenular axonal extension. In summary, local knockdown experiments indicate that Daam1a is required after 44 hpf in the habenular region for the growth of asymmetric neuropil and habenular efferent connectivity to the IPN.

Habenular overexpression of an activated form of DAAM1 increases the formation of neuropil and efferent connectivity to the IPN

To determine whether increased levels of Daam1a activity could promote habenular neuropil formation and axon extension, we performed local electroporation of a plasmid coding for a truncated form of DAAM1 that lacks the N-terminal regulatory domains (C-Daam1) and works as a dominant-positive (constitutively active) form (Fig. 3C) (Habas et al., 2001; Matusek et al., 2006; Ju et al., 2010). Local electroporation of *pcDNA-C-DAAM1-HA* in the habenular region at 44 hpf resulted in an ipsilateral increase of neuropil when directed to the L (Fig. 3D; n=8) but not to the R (supplementary material Fig. S6; n=9), compared with embryos electroporated with a control plasmid (data not shown; n=6), a finding that was corroborated by quantification of neuropil volume (L-Hb-C-DAAM1=14,473±119 μm^3; L-Hb-Co-plasmid=10,239±824 μm^3; P<0.05; n=5) (Fig. 3P,Q). By contrast to the differential effect in habenular neuropil growth, local electroporation of *pcDNA-DAAM1-HA* led to increase of *pou4f1-hsp70l:GFP* (+) habenular axons in the IPN when directed to either L (Fig. 3J,M) or R (supplementary material Fig. S6). In left-side-electroporated embryos, the volume of L Hb projections in the dIPN increased significantly (L-Hb-dIPN-C-DAAM1=36,147±818 μm^3; L-Hb-dIPN-Co-plasmid=27,603±1600 μm^3; P<0.05; n=3) whereas projections to the vIPN from either L or R Hb appeared unaffected (data not shown, P>0.05; n=3) (Fig. 3K,M). Habenular expression of *pou4f1-hsp70l:GFP* remained unchanged irrespective of the side (L, R or bilateral) of *pcDNA-C-DAAM1-HA* electroporation (Fig. 3G; supplementary material Fig. S6), indicating that habenular cell subtype organisation was unaffected. We thus conclude that over-activation of Daam1 in the habenular region, prior to and/or during the onset of neuropil and axonal morphogenesis, is sufficient to promote the growth of both habenular neuropil (when directed to the L) and axonal efferents to the IPN (when directed to either L or R).

Daam1a regulates dendritic and axonal outgrowth in individual habenular neurons

To assess directly whether dendritic and axonal outgrowth was sensitive to the modulation of Daam1a, we analysed the pattern of dendritic arborisation and shape of axonal terminals of individual habenular neurons labelled through focal electroporation of *pCS2:GAP43-GFP*. In control embryos, we recognised the stereotypical unipolar morphology of habenular neurons (Bianco et al., 2008), with a dense dendritic arbour (Fig. 4A, arrowheads) and a single unbranched axon extending from the soma (Fig. 4A, arrow; n=6). In addition, we observed the characteristic complex pattern of axon terminal morphology in the

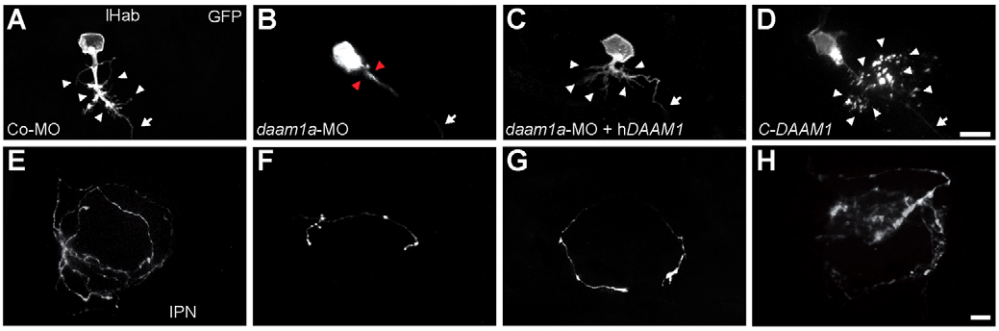

Fig. 4. Loss and gain of Daam1a function modulates dendritic growth and axonal terminal arborisation of dorsal habenular neurons. (**A**,**E**) Single habenular neuron from a control embryo showing the characteristic dense dendritic arborisation (A, arrowheads) and a single unbranched axon (A, arrow) that terminates in the IPN with complex bilateral spiral branches (E). (**B**,**F**) Single habenular neuron from a *daam1a-MO* embryo showing a pruned dendritic arbour (B, arrowheads) and a single axon (B, arrow) with incomplete and less complex organisation of axonal terminals in the IPN (F). (**C**,**G**) Single habenular neuron from an embryo co-injected with *daam1a-MO* and h*DAAM1*, showing normal dendritic arborisation (C, arrowheads) and partial rescue of axonal terminal morphology in the IPN (G). (**D**,**H**) Single habenular neuron from an embryo locally electroporated with *pcDNA-C-DAAM1-HA* at 44 hpf, showing increased dendritic arborisation (D, arrowheads) and axonal extension in the IPN (H). Images correspond to dorsal views of maximum intensity *z*-stack confocal projections of single neurons at 4.5 dpf, labelled through focal electroporation of *pCS2:GAP43-GFP*, with anterior to the top. Scale bars: 10 μm.

IPN, with bilateral and spiral branches (Fig. 4E) (Bianco et al., 2008). By contrast, habenular neurons from *daam1a-MO* embryos showed a greatly pruned dendritic arbour (Fig. 4B, arrowheads) and an incomplete and less complex pattern of axonal terminals in the IPN (Fig. 4F; *n*=5), compared with controls. Electroporated neurons from embryos co-injected with *daam1a-MO* and h*DAAM1* mRNA at the one- to two-cell stage developed a pattern of dendritic arborisation similar to controls (Fig. 4C, arrowheads) and showed a partial rescue of axonal terminal morphology in the IPN (Fig. 4G). Finally, habenular neurons from embryos locally electroporated with *pcDNA-C-DAAM1-HA* at 44 hpf showed increased dendritic arborisation (Fig. 4D, arrowheads) and axonal extension (Fig. 4H) in the IPN. Altogether, these findings corroborate that Daam1a regulates dendritic and axonal outgrowth in dorsal habenular neurons.

Daam1a is required for normal organisation of the cytoskeleton in the habenulae

As members of the Drf subfamily of Formin proteins act as actin assembly factors (Wallar and Alberts, 2003) and also play a less common role in regulating the stability of microtubules (Ju et al., 2010), we investigated whether the global loss of Daam1a function affected the organisation of F-actin and α-tubulin in the Hb. Embryos injected with Co-MO and co-stained with fluorescent phalloidin (to label F-actin) and Nissl (to delineate the cellular context of the Hb) showed a distinct smooth fibrillar organisation of F-actin in the Hb, with increased density of labelling in the asymmetric neuropil domains (Fig. 5A,D,G; *n*=12). By contrast, F-actin staining in the Hb of *daam1a-MO* embryos was irregular in shape and showed thicker and shorter bundles compared with controls (Fig. 5B,E,H; *n*=10). In these embryos, α-tubulin was also decreased and exhibited a less elaborate distribution than in controls (Fig. 5K,N,Q; *n*=10). Co-injection of *daam1a-MO* and h*DAAM1* mRNA resulted in partial rescue of the normal architecture of F-actin organisation in the Hb (Fig. 5C,F,I; *n*=10) and the strength of α-tubulin staining was increased (Fig. 5L,O,R; *n*=10). Altogether, these results indicate that Daam1a is required for the normal assembly and organisation of actin filaments in the developing zebrafish Hb, and also suggest a possible additional role for Daam1a in regulating microtubules.

Daam1a and Ulk2 collaborate in habenular neuropil morphogenesis

As the zebrafish Unc-51-like 2 (Ulk2) kinase has been recently implicated in the control of habenular neuropil morphogenesis downstream of Kctd proteins (Taylor et al., 2011), and the functional loss of Ulk2 induces a reduced habenular neuropil phenotype that resembles Daam1a knockdown (compare Fig. 6B and 6C), we investigated whether Daam1a and Ulk2 interact in the promotion of neuropil growth. Co-injection of morpholino directed against *daam1a* and *ulk2* (*ulk2*^{spl}*-MO*) at concentrations that in the context of single knockdowns induce only a modest reduction of habenular neuropil (Fig. 6D,E), led to severe reduction of habenular neuropil (Fig. 6F). Furthermore, h*DAAM1* mRNA rescued the habenular neuropil phenotype induced by loss of Ulk2 (Fig. 6H) whereas *ulk2* mRNA retained the habenular neuropil phenotype caused by knockdown of Daam1a (Fig. 6I). Altogether, these findings indicate that Daam1a and Ulk2 play a synergistic role in the promotion of neuropil growth, and that Daam1a is likely to work downstream of Ulk2 in the process.

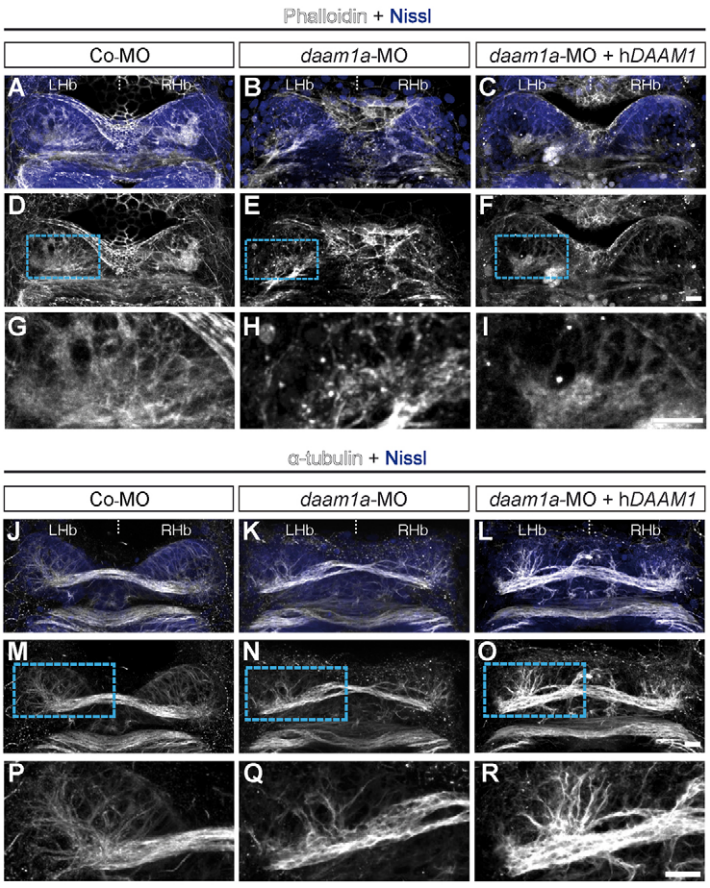

Fig. 5. Knockdown of Daam1a affects the organisation of filamentous actin and microtubules in the Hb. (**A**,**D**,**G**) The Hb of control embryos labelled with fluorescent phalloidin (F-actin, white) and counterstained with Nissl (to delineate the cellular context, purple) show a distinct smooth fibrillar organisation of F-actin, with increased compaction in the neuropil domains. (**B**,**E**,**H**) The Hb of *daam1a-MO* embryos show an irregular pattern of F-actin, with shorter and thicker bundles. (**C**,**F**,**I**) The Hb of embryos co-injected with *daam1a-MO* and h*DAAM1*, show a smooth fibrillar pattern of F-actin similar to controls. (**J**,**M**,**P**) The Hb of control embryos immunostained against α-tubulin (white) and counterstained with Nissl showed a distinct asymmetric distribution of α-tubulin corresponding to the neuropil domains. (**K**,**N**,**Q**) The Hb of *daam1a-MO* embryos show decreased and less elaborate α-tubulin staining. (**L**,**O**,**R**) The Hb of embryos co-injected with *daam1a-MO* and h*DAAM1*, show increased levels and thickness of α-tubulin (+) bundles than controls. G-I and P-R correspond to magnification views of the boxed regions in D-F and M-O, respectively. Images correspond to dorsal views of maximum intensity *z*-stack confocal projections, with anterior to the top. LHb, left Hb; RHb, right Hb. Scale bars: 20 μm.

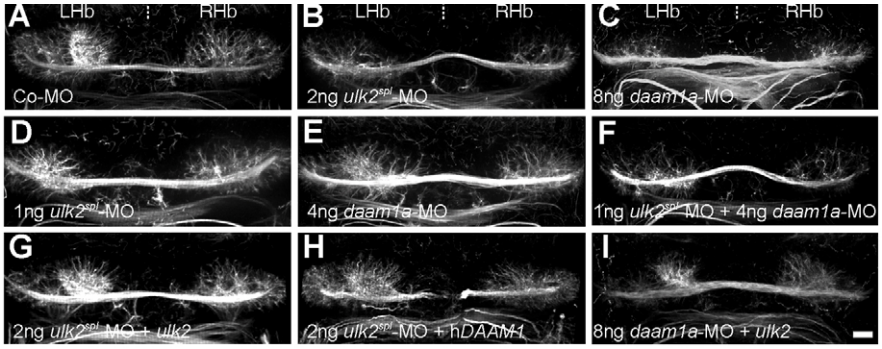

Fig. 6. Daam1a cooperates with Ulk2 in habenular neuropil formation. (**A-I**) The organisation of habenular neuropil at 4.5 hpf as revealed by anti acetylated α-tubulin immunostaining, after injection at the one- to four-cell stage with Co-MO (A), optimal doses of either *ulk2*^{spl}*-MO* (B, 2 ng) or *daam1a-MO* (C, 8 ng), suboptimal doses of either *ulk2*^{spl}*-MO* (D, 1 ng) or *daam1a-MO* (E, 4 ng), a combination of suboptimal doses of *ulk2*^{spl}*-MO* and *daam1a-MO* (F), optimal doses of *ulk2*^{spl}*-MO* (2 ng) combined with either *dUlk2* (G) or h*DAAM1* (H) mRNAs, or optimal dose of *daam1a-MO* (8 ng) combined with *ulk2* mRNA (I). Images correspond to dorsal views of maximum intensity confocal *z*-stack projections, with anterior to the top. LHb, left Hb; RHb, right Hb. Scale bar: 20 μm.

DISCUSSION

In this study, we used a reverse genetic approach to identify *daam1a* as a new genetic component of the pathways that control asymmetric habenular morphogenesis. Expression of *daam1a* in the developing Hb follows the specification of cell subtypes and mirrors the asymmetric changes in neuropil growth at embryonic and larval stages. Consistent with a role of Daam1a downstream of the main pathways that control the development of brain asymmetry (e.g. Fgf and Wnt) and its directionality (Nodal) in the brain, habenular daam1a expression becomes symmetric in *ace*$^{-/-}$ and *mbl*$^{-/-}$ mutants, and randomised after loss of Spaw or Ntl function. Importantly, loss and gain of Daam1a function decreases and increases, respectively, the formation of habenular neuropil and efferent axonal connectivity to the IPN without affecting habenular neurogenesis or cell subtype specification. These findings, and the fact that Daam1a promotes neuropil growth downstream of Ulk2, indicate that Daam1a plays a key role in asymmetric habenular morphogenesis, mediating the growth of habenular neuropil and efferent axonal connectivity to the IPN.

The opposite modulatory effect shown by loss and gain of Daam1a function in the ability to promote dendritic and axonal growth provides strong evidence in support of a role of Daam1a as a key modulator of neuronal morphogenesis in the Hb. The punctate distribution of Daam1a expression in the developing habenular neuropil, and more specifically in dendrites of habenular neurons, is also consistent with Daam1a participating in neuronal process outgrowth. Indeed, functional abrogation of Daam1a markedly disrupts the formation of dendritic processes examined in single habenular neurons, also leading to an incomplete and less complex pattern of axonal terminals in the IPN. Consistent with this, *Drosophila* Daam (dDaam) and mouse Daam1 (mDaam1) both regulate filopodial formation and neurite outgrowth in developing neurons (Matusek et al., 2008; Salomon et al., 2008; Gonçalves-Pimentel et al., 2011). dDaam shows a punctate distribution in F-actin-rich structures in the growth cones of cultured primary neurons (Matusek et al., 2008), whereas puncta of mDaam1 expression are observed in the dendritic shaft of pyramidal cells of the hippocampus, and in synaptic regions where Daam1 colocalises with pre-synaptic (Sv2) and post-synaptic (Psd95; also known as Dlg4) markers (Salomon et al., 2008). Importantly, d*Daam* is required for filopodial extension at axonal growth cones (Matusek et al., 2008; Gonçalves-Pimentel et al., 2011), whereas mDaam1 appears to play a role in dendritic extension (Salomon et al., 2008). In zebrafish, habenular neurons require Daam1a for both dendritic and axonal morphogenesis, although these two events appear to show differential Daam1a requirements, as they are affected to different extents after Daam1a knockdown (dendritic>axonal) and can be rescued to distinct degrees by overexpression of h*DAAM1* (again, dendritic>axonal). In addition, the extension of dendritic processes appears to be subject to local growth control depending on the side of the Hb. For example, local electroporation of *C-DAAM1* induces habenular neuropil growth only when directed to the L side, which suggests a mechanism that moderates the influence of Daam1 on neuropil growth in the R Hb, without affecting its ability to promote axonal extensions to the IPN. These results appear to be consistent with a recently proposed model of asymmetric local modulation of habenular neuropil growth mediated by Kctd proteins in zebrafish (Taylor et al., 2011). In this model, Kctd12.1 and Kctd12.2 are expressed primarily in the L and R Hb, respectively, and exert a stronger inhibition of neuropil growth on the R than the L Hb through interacting with Ulk2, a kinase that is expressed bilaterally in the Hb from 48 hpf (Taylor et al., 2011). Whether Kctd proteins inhibit the ability of Daam1a to promote neuropil growth in the R Hb is yet to be determined. However, the onset of asymmetric *daam1a* expression coincides with the onset of *ulk2* expression and both are concurrent with neuropil growth in the Hb, suggesting a link between these events. Indeed, Daam1a and Ulk2 play a synergistic role in the promotion of neuropil growth. Furthermore, h*DAAM1* overexpression rescues the impaired neuropil phenotype induced by functional loss of Ulk2 (whereas Ulk2 appears to be unable to rescue the phenotype induced by Daam1a knockdown) suggesting that Daam1a works downstream of Ulk2. Altogether, these findings are consistent with a collaborative role of Daam1a and Ulk2 in the promotion of neuropil growth downstream of the pathways that establish cell subtype specification in the Hb. Where and how such collaboration occurs remains to be determined. An intriguing possibility is the endocytic pathway, as Ulk1 and Ulk2 localise to vesicular structures in growth cones and regulate neuronal process extension through early endosome trafficking at nascent neurites (Tomoda et al., 2004; Zhou et al., 2007; Toda et al., 2008), whereas zebrafish Daam1a is actively transported to endocytic vesicles and its asymmetric subcellular localisation appears to be relevant for the convergent-extension movements of notochordal cells (Kida et al., 2007).

At the effector level, Daam1a regulates both F-actin and microtubule assembly during habenular morphogenesis. The former role is consistent with previous reports indicating that Daam1 works as an F-actin nucleation and elongation factor induced by Rho GTPases (Prokop et al., 2011), and that dDaam cooperates with Arp2 and Arp3 in a common mechanism of filopodia formation that depends on Enabled and is regulated through Profilin (Chickadee – FlyBase) activity (Gonçalves-Pimentel et al., 2011). Reports linking Daam1 to microtubule assembly and stabilisation are, however, scarce (Ju et al., 2010). The observed increase in intensity of α-tubulin (+) labelling after expression of h*DAAM1* suggests that zebrafish Daam1a regulates microtubule dynamics in the Hb. Regulation of F-actin and microtubule dynamics might result from Daam1a interacting with other signalling pathways, such as Wnt/PCP signalling, which is known to modulate the growth of axons and dendrites (Wang and Nathans, 2007; Tissir and Goffinet, 2010). Daam1 works as an intermediary of Wnt/PCP signalling that leads to Rho activation and subsequent remodelling of the cytoskeleton during *Xenopus* and zebrafish gastrulation (Habas et al., 2001; Kida et al., 2007), and some ligands and core components of Wnt/PCP are expressed in the developing Hb at the time of neuropil formation (data not shown).

Here, we demonstrate that Daam1a plays a key role in asymmetric habenular morphogenesis by regulating dendritic and axonal outgrowth in dorsal habenular neurons, possibly through the modulation of cytoskeletal dynamics. Although Daam1 and Ulk2 have a synergistic role in the promotion of habenular neuropil growth, downstream of the pathways that establish asymmetric cell subtype specification, further studies are needed to address how these two factors interact and become differentially modulated on L and R sides of the Hb.

Acknowledgements
We thank Ricardo Armisen for critical reading of the manuscript; Drs Raymond Habas and Joshua Gamse for providing plasmids; members of the Laboratory of Experimental Ontogeny Fish Facility for fish care; Erika Labbe and Jorge Jara for technical help with image processing; Carmen Gloria Lemus for advice in the statistical approach; and Luis Michea for sharing the use of the qPCR machine.

Funding
This work was supported by the Howard Hughes Medical Institute (to M.L.C.), The National Fund for Scientific and Technological Development (FONDECYT) [1109324 to A.C., 1120579 to S.H. and 1120558 to M.L.C.]; the Commission of the European Communities [FP6-2004-NEST-PATH EDCBNL to M.L.C. and S.W.W.]; the Scientific Millennium Initiative [P09-015-F to M.L.C. and S.H.]; and the Wellcome Trust [S.W.W. and M.C.]. Deposited in PMC for immediate release.

Competing interests statement
The authors declare no competing financial interests.

Author contributions
A.C. participated in the design of the study; performed SSH, library hybridisation, *in situ* hybridisation screening, clone selection, and morpholino and mRNA injections; helped in the supervision of the study; wrote early drafts of the manuscript; and provided comments and revisions on further versions. K.P. carried out most immunostaining and prepared most figures. L.A. and M.M.M. performed local and focal electroporation, and processed the images of these experiments. M.M. designed the SSH protocol and helped in performing SHH. I.S. carried out actin/tubulin immunostaining, prepared figures and provided comments on the manuscript. C.M. carried out *in situ* hybridisation, anti-HuC/D inmunostaining and the determination of habenular cell number and neuropil volume. N.G. performed lipophilic labelling of habenular efferent connectivity. R.P. carried out qPCR experiments. J.S and K.M. helped with data analysis and provided comments on the writting. S.H. and L.B. performed neuropil and IPN volume data analyses. S.W.W. provided lab support at early stages of the reverse genetics approach and revisons/comments on later versions of the manuscript. M.L.C. conceived and supervised the project, and wrote the manuscript.

Supplementary material
Supplementary material available online at
http://dev.biologists.org/lookup/suppl/doi:10.1242/dev.091934/-/DC1

References
Agetsuma, M., Aizawa, H., Aoki, T., Nakayama, R., Takahoko, M., Goto, M., Sassa, T., Amo, R., Shiraki, T., Kawakami, K. et al. (2010). The habenula is crucial for experience-dependent modification of fear responses in zebrafish. *Nat. Neurosci.* **13**, 1354-1356.
Aizawa, H., Bianco, I. H., Hamaoka, T., Miyashita, T., Uemura, O., Concha, M. L., Russell, C., Wilson, S. W. and Okamoto, H. (2005). Laterotopic representation of left-right information onto the dorso-ventral axis of a zebrafish midbrain target nucleus. *Curr. Biol.* **15**, 238-243.
Aizawa, H., Goto, M., Sato, T. and Okamoto, H. (2007). Temporally regulated asymmetric neurogenesis causes left-right difference in the zebrafish habenular structures. *Dev. Cell* **12**, 87-98.
Aizawa, H., Amo, R. and Okamoto, H. (2011). Phylogeny and ontogeny of the habenular structure. *Front Neurosci* **5**, 138.
Bianco, I. H. and Wilson, S. W. (2009). The habenular nuclei: a conserved asymmetric relay station in the vertebrate brain. *Philos. Trans. R. Soc. B* **364**, 1005-1020.
Bianco, I. H., Carl, M., Russell, C., Clarke, J. D. and Wilson, S. W. (2008). Brain asymmetry is encoded at the level of axon terminal morphology. *Neural Dev.* **3**, 9.
Bisgrove, B. W., Essner, J. J. and Yost, H. J. (1999). Regulation of midline development by antagonism of lefty and nodal signaling. *Development* **126**, 3253-3262.
Burgess, H. A., Johnson, S. L. and Granato, M. (2009). Unidirectional startle responses and disrupted left-right co-ordination of motor behaviors in robo3 mutant zebrafish. *Genes Brain Behav.* **8**, 500-511.
Carl, M., Bianco, I. H., Bajoghli, B., Aghaallaei, N., Czerny, T. and Wilson, S. W. (2007). Wnt/Axin1/beta-catenin signaling regulates asymmetric nodal activation, elaboration, and concordance of CNS asymmetries. *Neuron* **55**, 393-405.
Concha, M. L. (2004). The dorsal diencephalic conduction system of zebrafish as a model of vertebrate brain lateralisation. *Neuroreport* **15**, 1843-1846.
Concha, M. L. and Wilson, S. W. (2001). Asymmetry in the epithalamus of vertebrates. *J. Anat.* **199**, 63-84.
Concha, M. L., Burdine, R. D., Russell, C., Schier, A. F. and Wilson, S. W. (2000). A nodal signaling pathway regulates the laterality of neuroanatomical asymmetries in the zebrafish forebrain. *Neuron* **28**, 399-409.
Concha, M. L., Russell, C., Regan, J. C., Tawk, M., Sidi, S., Gilmour, D. T., Kapsimali, M., Sumoy, L., Goldstone, K., Amaya, E. et al. (2003). Local tissue interactions across the dorsal midline of the forebrain establish CNS laterality. *Neuron* **39**, 423-438.
Concha, M. L., Signore, I. A. and Colombo, A. (2009). Mechanisms of directional asymmetry in the zebrafish epithalamus. *Semin. Cell Dev. Biol.* **20**, 498-509.
Concha, M. L., Bianco, I. H. and Wilson, S. W. (2012). Encoding asymmetry within neural circuits. *Nat. Rev. Neurosci.* **13**, 832-843.
Essner, J. J., Branford, W. W., Zhang, J. and Yost, H. J. (2000). Mesendoderm and left-right brain, heart and gut development are differentially regulated by pitx2 isoforms. *Development* **127**, 1081-1093.
Facchin, L., Burgess, H. A., Siddiqi, M., Granato, M. and Halpern, M. E. (2009). Determining the function of zebrafish epithalamic asymmetry. *Philos. Trans. R. Soc. B* **364**, 1021-1032.
Feldman, B. and Stemple, D. L. (2001). Morpholino phenocopies of sqt, oep, and ntl mutations. *Genesis* **30**, 175-177.
Gamse, J. T., Thisse, C., Thisse, B. and Halpern, M. E. (2003). The parapineal mediates left-right asymmetry in the zebrafish diencephalon. *Development* **130**, 1059-1068.
Gamse, J. T., Kuan, Y. S., Macurak, M., Brösamle, C., Thisse, B., Thisse, C. and Halpern, M. E. (2005). Directional asymmetry of the zebrafish epithalamus guides dorsoventral innervation of the midbrain target. *Development* **132**, 4869-4881.
Gilmour, D. T., Maischein, H. M. and Nüsslein-Volhard, C. (2002). Migration and function of a glial subtype in the vertebrate peripheral nervous system. *Neuron* **34**, 577-588.
Gonçalves-Pimentel, C., Gombos, R., Mihály, J., Sánchez-Soriano, N. and Prokop, A. (2011). Dissecting regulatory networks of filopodia formation in a Drosophila growth cone model. *PLoS ONE* **6**, e18340.
Gubler, U. and Hoffman, B. J. (1983). A simple and very efficient method for generating cDNA libraries. *Gene* **25**, 263-269.
Habas, R., Kato, Y. and He, X. (2001). Wnt/Frizzled activation of Rho regulates vertebrate gastrulation and requires a novel Formin homology protein Daam1. *Cell* **107**, 843-854.

Heisenberg, C. P., Houart, C., Take-Uchi, M., Rauch, G. J., Young, N., Coutinho, P., Masai, I., Caneparo, L., Concha, M. L., Geisler, R. et al. (2001). A mutation in the Gsk3-binding domain of zebrafish Masterblind/Axin1 leads to a fate transformation of telencephalon and eyes to diencephalon. *Genes Dev.* **15**, 1427-1434.
Hendricks, M. and Jesuthasan, S. (2007a). Asymmetric innervation of the habenula in zebrafish. *J. Comp. Neurol.* **502**, 611-619.
Hendricks, M. and Jesuthasan, S. (2007b). Electroporation-based methods for in vivo, whole mount and primary culture analysis of zebrafish brain development. *Neural Dev.* **2**, 6.
Jesuthasan, S. (2011). Fear, anxiety and control in the zebrafish. *Dev. Neurobiol.*
Ju, R., Cirone, P., Lin, S., Griesbach, H., Slusarski, D. C. and Crews, C. M. (2010). Activation of the planar cell polarity formin DAAM1 leads to inhibition of endothelial cell proliferation, migration, and angiogenesis. *Proc. Natl. Acad. Sci. USA* **107**, 6906-6911.
Kida, Y. S., Sato, T., Miyasaka, K. Y., Suto, A. and Ogura, T. (2007). Daam1 regulates the endocytosis of EphB during the convergent extension of the zebrafish notochord. *Proc. Natl. Acad. Sci. USA* **104**, 6708-6713.
Kimmel, C. B., Ballard, W. W., Kimmel, S. R., Ullmann, B. and Schilling, T. F. (1995). Stages of embryonic development of the zebrafish. *Dev. Dyn.* **203**, 253-310.
Lee, A., Mathuru, A. S., Teh, C., Kibat, C., Korzh, V., Penney, T. B. and Jesuthasan, S. (2010). The habenula prevents helpless behavior in larval zebrafish. *Curr. Biol.* **20**, 2211-2216.
Liu, W., Sato, A., Khadka, D., Bharti, R., Diaz, H., Runnels, L. W. and Habas, R. (2008). Mechanism of activation of the Formin protein Daam1. *Proc. Natl. Acad. Sci. USA* **105**, 210-215.
Long, S., Ahmad, N. and Rebagliati, M. (2003). The zebrafish nodal-related gene southpaw is required for visceral and diencephalic left-right asymmetry. *Development* **130**, 2303-2316.
Matusek, T., Djiane, A., Jankovics, F., Brunner, D., Mlodzik, M. and Mihály, J. (2006). The Drosophila formin DAAM regulates the tracheal cuticle pattern through organizing the actin cytoskeleton. *Development* **133**, 957-966.
Matusek, T., Gombos, R., Szécsényi, A., Sánchez-Soriano, N., Czibula, A., Pataki, C., Gedai, A., Prokop, A., Raskó, I. and Mihály, J. (2008). Formin proteins of the DAAM subfamily play a role during axon growth. *J. Neurosci.* **28**, 13310-13319.
Miyasaka, N., Morimoto, K., Tsubokawa, T., Higashijima, S., Okamoto, H. and Yoshihara, Y. (2009). From the olfactory bulb to higher brain centers: genetic visualization of secondary olfactory pathways in zebrafish. *J. Neurosci.* **29**, 4756-4767.
Parinov, S., Kondrichin, I., Korzh, V. and Emelyanov, A. (2004). Tol2 transposon-mediated enhancer trap to identify developmentally regulated zebrafish genes in vivo. *Dev. Dyn.* **231**, 449-459.
Prokop, A., Sánchez-Soriano, N., Gonçalves-Pimentel, C., Molnár, I., Kalmár, T. and Mihály, J. (2011). DAAM family members leading a novel path into formin research. *Commun. Integr. Biol.* **4**, 538-542.
Regan, J. C., Concha, M. L., Roussigne, M., Russell, C. and Wilson, S. W. (2009). An Fgf8-dependent bistable cell migratory event establishes CNS asymmetry. *Neuron* **61**, 27-34.
Reifers, F., Böhli, H., Walsh, E. C., Crossley, P. H., Stainier, D. Y. and Brand, M. (1998). Fgf8 is mutated in zebrafish acerebellar (ace) mutants and is required for maintenance of midbrain-hindbrain boundary development and somitogenesis. *Development* **125**, 2381-2395.
Roussigné, M., Bianco, I. H., Wilson, S. W. and Blader, P. (2009). Nodal signalling imposes left-right asymmetry upon neurogenesis in the habenular nuclei. *Development* **136**, 1549-1557.
Roussigné, M., Blader, P. and Wilson, S. W. (2011). The zebrafish epithalamus clears a path through the complexity of brain lateralization. *Dev. Neurobiol.* **72**, 269-281.
Salomon, S. N., Haber, M., Murai, K. K. and Dunn, R. J. (2008). Localization of the Diaphanous-related formin Daam1 to neuronal dendrites. *Neurosci. Lett.* **447**, 62-67.
Schmittgen, T. D. and Livak, K. J. (2008). Analyzing real-time PCR data by the comparative C(T) method. *Nat. Protoc.* **3**, 1101-1108.
Signore, I. A., Guerrero, N., Loosli, F., Colombo, A., Villalón, A., Wittbrodt, J. and Concha, M. L. (2009). Zebrafish and medaka: model organisms for a comparative developmental approach of brain asymmetry. *Philos. Trans. R. Soc. B* **364**, 991-1003.
Tawk, M., Bianco, I. H. and Clarke, J. D. (2009). Focal electroporation in zebrafish embryos and larvae. *Methods Mol. Biol.* **546**, 145-151.
Taylor, R. W., Qi, J. Y., Talaga, A. K., Ma, T. P., Pan, L., Bartholomew, C. R., Klionsky, D. J., Moens, C. B. and Gamse, J. T. (2011). Asymmetric inhibition of Ulk2 causes left-right differences in habenular neuropil formation. *J. Neurosci.* **31**, 9869-9878.
Thisse, C. and Thisse, B. (2008). High-resolution in situ hybridization to whole-mount zebrafish embryos. *Nat. Protoc.* **3**, 59-69.
Tissir, F. and Goffinet, A. M. (2010). Planar cell polarity signaling in neural development. *Curr. Opin. Neurobiol.* **20**, 572-577.
Toda, H., Mochizuki, H., Flores, R., 3rd, Josowitz, R., Krasieva, T. B., Lamorte, V. J., Suzuki, E., Gindhart, J. G., Furukubo-Tokunaga, K. and Tomoda, T. (2008). UNC-51/ATG1 kinase regulates axonal transport by mediating motor-cargo assembly. *Genes Dev.* **22**, 3292-3307.
Tomoda, T., Kim, J. H., Zhan, C. and Hatten, M. E. (2004). Role of Unc51.1 and its binding partners in CNS axon outgrowth. *Genes Dev.* **18**, 541-558.
Wallar, B. J. and Alberts, A. S. (2003). The formins: active scaffolds that remodel the cytoskeleton. *Trends Cell Biol.* **13**, 435-446.
Wang, Y. and Nathans, J. (2007). Tissue/planar cell polarity in vertebrates: new insights and new questions. *Development* **134**, 647-658.
Zhou, X., Babu, J. R., da Silva, S., Shu, Q., Graef, I. A., Oliver, T., Tomoda, T., Tani, T., Wooten, M. W. and Wang, F. (2007). Unc-51-like kinase 1/2-mediated endocytic processes regulate filopodia extension and branching of sensory axons. *Proc. Natl. Acad. Sci. USA* **104**, 5842-5847.

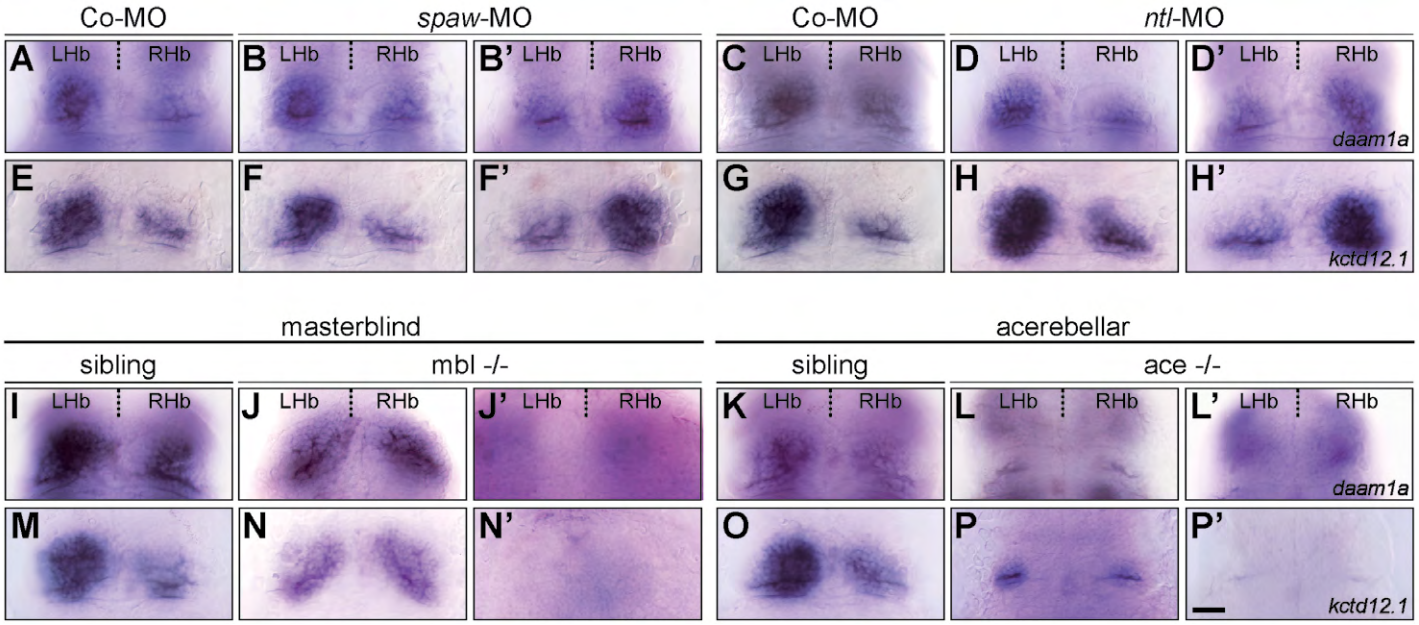

Fig. S1. Habenular expression of daam1a and kcdt12.1 in embryos with affected habenular asymmetry. (**A**,**C**,**I**,**K**) Habenular expression of daam1a in embryos injected with Co-MO (A,C) and in siblings of masterblind (mbl) (I) and acerebellar (ace) (K) mutants. (**E**,**G**,**M**,**O**) Habenular expression of kcdt12.1 in embryos injected with Co-MO (E,G) and in siblings of mbl (M) and ace (O) mutants. (**B**,**B′**,**F**,**F′**) Injection of spaw-MO results in randomised laterality of habenular daam1a (B,B′) and kcdt12.1 (F,F′) asymmetric expression. (**D**,**D′**,**H**,**H′**) Injection of ntl-MO results in randomised laterality of habenular daam1a (D,D′) and kcdt12.1 (H,H′) asymmetric expression. (**J**,**J′**,**N**,**N′**) $mbl^{-/-}$ mutants show symmetric expression of daam1a (J) and kcdt12.1 (N), with both sides showing levels similar to the right Hb of controls; some embryos also show absence of expression (J′,N′). (**L**,**L′**,**P**,**P′**) $ace^{-/-}$ mutants show symmetric expression of daam1a (L) and kcdt12.1 (P), with both sides showing levels similar to the right Hb of controls; some embryos also show absence of expression (L′,P′). The relative contribution of the different phenotypes is given in Table 1. Images correspond to dorsal views of the habenular region at 96 hpf, with anterior to the top. Scale bar, 20 μm.

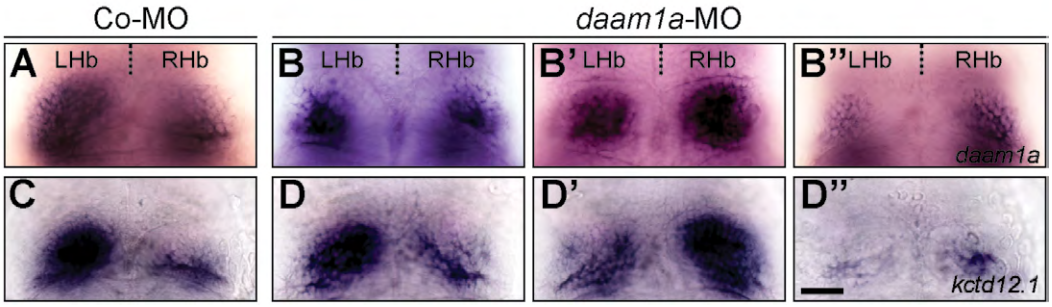

Fig. S2. Habenular expression of *daam1a* and kctd12.1 after Daam1a knock-down. (**A**,**C**) Expression of daam1a (A) and kcdt12.1 (C) in control embryos, revealing the enlarged asymmetric domain of the left Hb. (**B-B′′**) Global knock down of Daam1a results in equal proportions of asymmetric left-sided (B), asymmetric right-sided (B′), and bilateral-right symmetric (B′′) expression of daam1a. (**D-D′′**) Global knock down of Daam1a leads to equal proportions of asymmetric left-sided (D), asymmetric right-sided (D′), and bilateral-right symmetric (D′′) expression of kcdt12.1. The relative contributions of the different phenotypes are given in Table 2. Images correspond to dorsal views of the habenular region at 96 hpf, with anterior to the top. Scale bar, 20 μm.

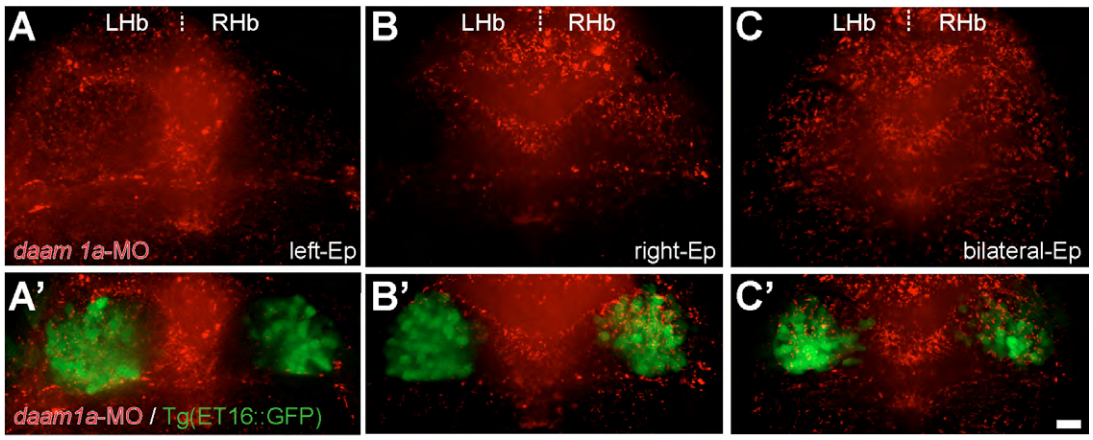

Fig. S3. Efficiency of daam1a-MO local electroporation (Ep) in the habenular region. (**A-C′**) Distribution of lissamine-tagged daam1a-MO (red) locally electroporated into the left (A,A′), right (B,B′) and bilateral (C,C′) habenular regions (green) of Tg(ET16::GFP) embryos. Images correspond to dorsal views of maximum intensity z-stack confocal projections, with anterior to the top. Scale bar, 20 µm.

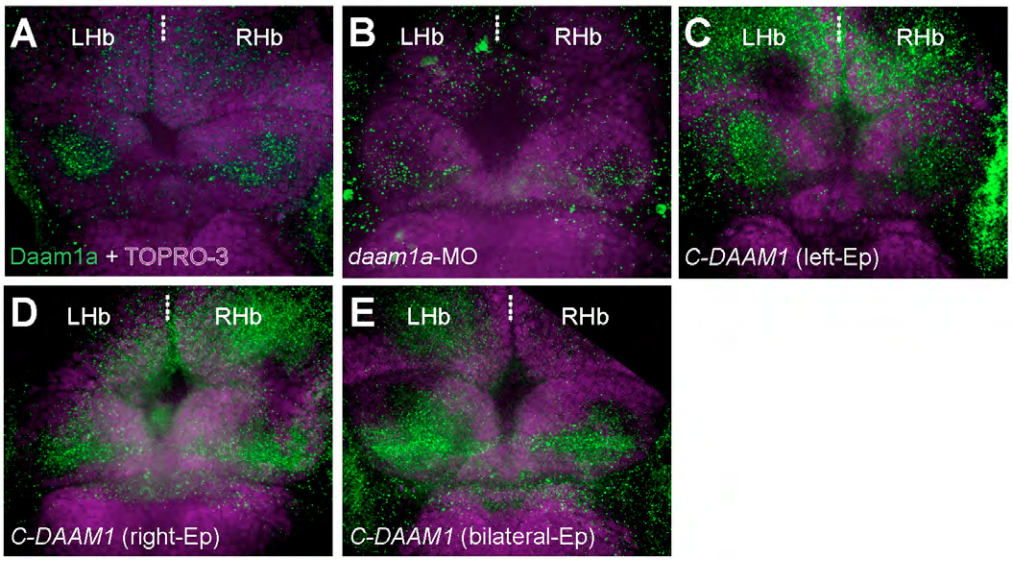

Fig. S4. Changes in the relative levels of the endogenous Daam1a protein after local electroporation (Ep). (**A**) The Hb of control embryos labelled through indirect immunofluorescence against Daam1a (green) and counter stained with TO-PRO-3 to delineate the cellular context of the Hb (purple) showed a distinct punctate expression of Daam1a in the habenular neuropil, larger on the left compared to the right side at 96 hpf. (**B**) The Hb of embryos subjected to left-sided local electroporation of daam1a-MO show decreased levels of Daam1a expression at 96 hpf, primarily on the left Hb. (**C**) The Hb of embryos subjected to left-sided local electroporation of *C-DAAM1* showed increased levels of Daam1a expression in the left Hb at 96 hpf. (**D**) The Hb of embryos after right-sided local electroporation of *C-DAAM1* showed increase expression levels of Daam1a in the right Hb at 96 hpf, compared to controls. (**E**) The Hb of embryos subjected to bilateral local electroporation of *C-DAAM1* showed increased levels of Daam1a expression in both left and right Hb at 96 hpf. Images correspond to dorsal views of maximum intensity z-stack confocal projections, with anterior to the top. Scale bar, 20 µm.

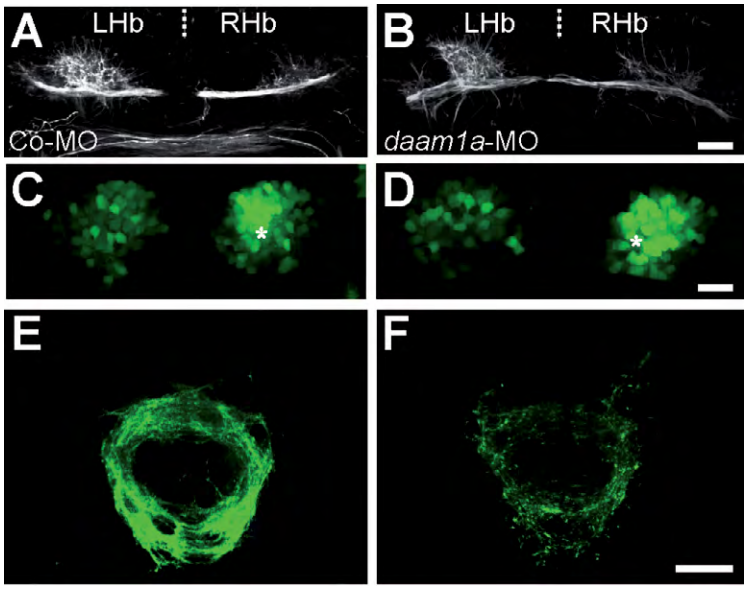

Fig. S5. Bilateral electroporation of daam1a-MO induces defects in neuropil formation and IPN connectivity. (**A-F**) Dorsal views of maximum intensity z-stack confocal projections of the habenular region (A-D) and IPN (E,F) in Tg(pou4f1-hsp70l:GFP) embryos at 4.5 dpf, with anterior to the top. The habenular neuropil was immunostained against acetylated α-tubulin (A,B, white), while the soma (C,D) and efferent projections (E,F) of dorsal habenular neurons expressing pou4f1-hsp70l:GFP were detected in vivo (green). Each column corresponds to a different condition of local electroporation: control-MO (left) and daam1a-MO (right). Asterisks in C and D indicate the enlarged cellular domain of the Hb expressing the pou4f1-hsp70l:GFP transgene. Scale bar, 20µm.

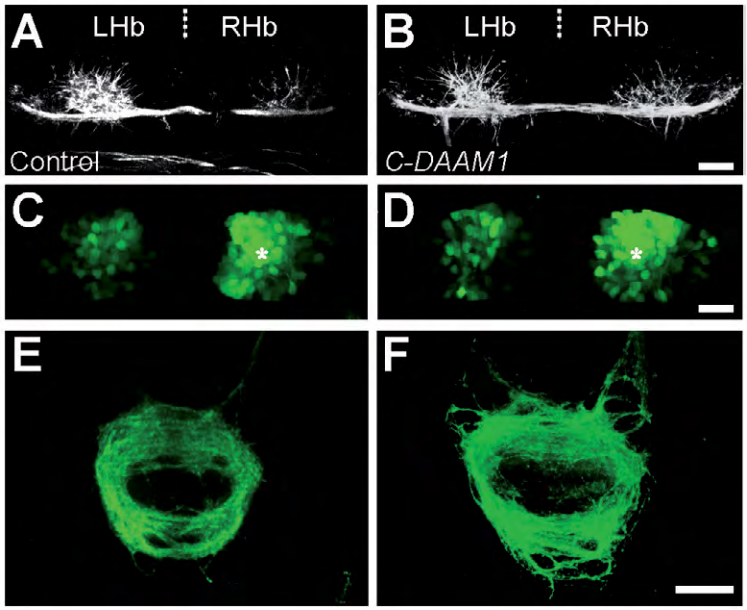

Fig. S6. Local electroporation of *C-DAAM1* in the right habenular region induces increased axonal efferent connectivity to the IPN, without affecting habenular neuropil. (**A-F**) Dorsal views of maximum intensity z-stack confocal projections of the habenular region (A-D) and IPN (E,F) in Tg(pou4f1-hsp70l:GFP) embryos at 4.5 dpf, with anterior to the top. The habenular neuropil was immunostained against acetylated α-tubulin (A,B, white), while the soma (C,D) and efferent projections (E,F) of dorsal habenular neurons expressing pou4f1-hsp70l:GFP were detected in vivo (green). Each column corresponds to a different condition of local electroporation: control plasmid (left) and *pcDNA-C-DAAM1-HA* (right). Asterisks in C and D indicate the enlarged cellular domain of the Hb expressing the pou4f1-hsp70l:GFP transgene. Scale bar, 20µm.